

# Pathways to faceting of vesicles

Mark Bowick\* and Rastko Sknepnek†

*Department of Physics, Syracuse University, Syracuse, New York 13244, USA*

An interplay between geometry, topology, and order can lead to geometric frustration that profoundly affects the shape and structure of a curved surface. In this paper we discuss how such effects can result in faceting of elastic vesicles. We show that under the right conditions an assortment of regular and irregular polyhedral structures can be the low energy states of such elastic objects. In particular, we discuss how topological defects necessarily present in any crystalline lattice confined to spherical topology naturally lead to the formation of icosahedra in a homogeneous elastic vesicle. Furthermore, we show that introducing heterogeneities in the elastic properties or allowing for a non-linear bending response of a homogeneous system opens non-trivial pathways to the formation of faceted, yet non-icosahedral structures.

## I. INTRODUCTION

While most of the lipid bilayer vesicles found in biological systems are smooth, this is not always the case and one often observes faceted structures. Prominent examples in the nature are protein capsids of some viruses, bacterial organelles carboxysomes,<sup>1</sup> and square-shaped bacteria found in saturated brine pools.<sup>2</sup> On the experimental side faceted forms are found in small phosphatidylcholine vesicles below the freezing temperature,<sup>3</sup> some cationic vesicles,<sup>4,5</sup> cross-polymerized vesicles,<sup>6</sup> vesicles assembled from a mixture of anionic and cationic amphiphiles,<sup>5,7,8</sup> vesicles formed from block copolymers with liquid-crystalline side chains,<sup>9–11</sup> giant fullerenes,<sup>12</sup> and gold nanocages.<sup>13</sup> While very different in their structure, all these systems share the common feature of possessing pathways to lower the total energy by forming stable facets. Over the past four decades a substantial research effort has been devoted to understanding the shapes of smooth vesicles. Only in the past couple of years there has been growing interest in developing theoretical understanding of the faceted structures.

To understand the origin of faceting it is essential to understand the physics of smooth vesicles. Early in evolution it became clear that in order to construct complex life it was necessary to be able to hierarchically compartmentalize and separate different parts of an organism. The compartmentalization was achieved with the aid of vesicles made of thin membranes. Biological membranes are typically lipid bilayer structures interpenetrated with a variety of membrane and transmembrane proteins.<sup>14</sup> They are usually very thin ( $\sim 5\text{nm}$ ) compared to their lateral dimensions (tens to hundreds of nanometers to microns) and thus quasi-two-dimensional. While being ubiquitous in living organisms, vesicular membranes are not limited to biological systems. Nano- and micro-size containers can be constructed in the laboratory using

lipid molecules,<sup>15,16</sup> block-copolymers<sup>17</sup> and even inorganic compounds, as in the case of gold nanocages.

While the detailed structure and function of biological membranes is exceedingly complex and not fully understood, much insight into their physical properties can be gained by constructing simple mesoscopic models. In a seminal paper, Helfrich<sup>18</sup> argued that due to its quasi-two-dimensional nature the dominant deformation of a membrane is bending. Therefore it can be qualitatively described in terms of changes of the membrane's curvature. He constructed a free energy functional that relates the bending energy to the integral of the square of the mean curvature,  $H$ , and to the Gaussian curvature,  $K$ , i.e.,

$$E_{\text{bend}} = \int dS \left[ 2\kappa (H - H_0)^2 + \kappa_G K \right], \quad (1)$$

where  $H_0$  is the spontaneous curvature and  $\kappa$  and  $\kappa_G$  are material-dependent bending and Gaussian rigidities. It is evident that the Helfrich free does not account for any change in the energy due to stretching or shear deformations. In other words, it is suitable for describing fluid membranes where molecules are confined to the membrane surface but are free to laterally diffuse within it. Fluidity is important for biological membranes as it ensures that small apertures formed by transmembrane transport or as a result of a damage can quickly be closed; it also allows structural reorganizations within the membrane itself, as in the case, for example, of lipid rafts.<sup>19</sup>

Homogeneous fluid vesicles are typically smooth as molecules quickly rearrange themselves to remove any stress that would be generated by the formation of sharp corners and edges. Sharp structures represent regions with diverging curvature<sup>20</sup> and are therefore energetically costly. While in real systems the actual divergence is cut off at some molecular length scale, the energy penalty for forming sharp turns is comparable to the molecular energies and far exceeds any energy penalty for forming long-wavelength undulations that are  $\sim k_B T$ . In

order to form sharp structures, therefore, it is necessary to have a mechanism that would either reduce the energy cost associated with the formation of bends or prevent the flow of the molecules or impose additional “in-vesicle” order (e.g., liquid crystalline) that would dictate the underlying geometry. The former can be achieved by asymmetry in the composition between two leaflets of the bilayer induced by a phase segregation of the two molecular species, thus resulting in local non-zero spontaneous curvature<sup>21</sup> or by segregating excess amphiphiles along long ridges and inducing a spontaneous curvature that is commensurate with the dihedral angle between two faces.<sup>7,22</sup> In this paper we discuss mechanisms that lead to faceting of solid (crystalline) vesicles.

This paper is organized as follows. In Section II A we discuss pathways to the faceting of elastic (tethered) membranes that describe viral capsids or bilayer systems cooled below the gelation transition or for which the molecules are cross-polymerized (i.e., tethered to each other). In particular, in Section II A we show how topological defects can act as the seeds of buckling into icosahedra providing a simple explanation for the observation that viruses with icosahedral symmetry take spherical shape if their radius is small but are well faceted icosahedra if they are larger in size. In Section II B we show how the presence of elastic inhomogeneities also can lead to faceting into regular and irregular polyhedra different from the ubiquitous icosahedron. Finally, in Section II C we argue that faceting can also occur in homogeneous elastic vesicles if one allows for non-linear bending response in terms of a critical curvature.

## II. FACETING OF ELASTIC MEMBRANES

### A. Buckling into icosahedra

One of the hallmarks of viruses is a regular structure of the capsid. The unit building blocks of the capsid are capsomeres, robust protein complexes,  $\approx 10\text{nm}$  in diameter that tile the capsid in a crystalline array. Lattice structures of icosahedral viruses can be described in terms of pairs of non-negative integers,  $(p, q)$  that form a  $T$ -number,  $T = p^2 + q^2 + pq$ .<sup>23</sup> The existence of a lattice combined with the spherical topology is at the center of the argument for size-driven buckling into icosahedra. In order to explain the mechanism behind this buckling phenomenon we first need to briefly review the complex question of the existence of long-range order in curved spaces.

Constructing a regular lattice in a plane (or any other zero Gaussian curvature surface) is fairly easy.

The simplest example is the ground state of identical point-like particles in an external confining potential interacting via long range repulsive interactions, e.g., identical charges confined to a planar region. The ground state is a triangular lattice with each particle having exactly six equidistant nearest neighbors and a lattice constant that is determined by the density. Such a state is not frustrated and is stress free. This is no longer the case when one tries to perform a similar construction on the surface of a sphere. Any attempt to map a regular lattice onto a surface of the sphere will result in an excess of particles and their mutual overlap. In other words, in order to build smooth covering of a sphere it is necessary to remove parts of the original planar lattice. As a result, even in the ground state any crystalline lattice on a sphere will necessarily have a finite number of sites that have coordination different than six, i.e., so called topological defects. Starting from the Euler’s polyhedral formula (after all a tiling of a sphere can be thought of as a polyhedron!) which states that for any polyhedron  $V - E + F = \chi$ , where  $V$  is the number of vertices,  $E$  is the number of edges,  $F$  is the number of faces, and  $\chi$  is the Euler characteristic of the polyhedron, one can show that the total number of vertices of a crystalline lattice on a sphere has to satisfy the following relation:<sup>24</sup>  $\sum_z (6 - z) N_z = 6\chi = 12$ .  $N_z$  is the total number of sites with coordination  $z$  and we have explicitly used that for a sphere  $\chi = 2$ . The configuration with the lowest number of defects on a sphere is  $N_5 = 12$ , i.e., twelve five-fold coordinated sites embedded in a regular triangular lattice. We note that, somewhat counterintuitively, this configuration is not always the ground state of the system as shown by Bowick, *et al.*:<sup>25</sup> for reasonable defect core energies the total energy can be lowered by forming pairs of five- and seven-fold defects that emanate from each of the twelve five-fold coordinated sites. In the following discussion we will ignore this complication and assume that only twelve five-fold defects are present.

Despite their appearance five-fold disclination defects are not local since they owe their existence to removing whole sections of a planar lattice so that it conforms to the surface of a sphere. As such they are endowed with considerable elastic energy. To estimate how the elastic energy of a disclination depends on its size we assume that it is surrounded by a Hookean elastic medium. The elastic energy of a two-dimensional crystal is<sup>26</sup>  $E_{el} = \int d^2\vec{r} A^{ijkl} u_{ij} u_{kl}$ , where  $u_{ij}(\vec{r}) = \frac{1}{2}(\partial_i u_j + \partial_j u_i + \partial_k u_i \partial_k u_j)$  is the strain tensor field with  $u_i(\vec{r})$  ( $i = 1, 2$ ) being components of the displacement field and  $A^{ijkl}$  is the material-dependent elastic tensor. For a hexagonal lattice, the elastic tensor has only two independent components,<sup>26</sup> i.e., two Lamé coefficients  $\mu$  and  $\lambda$

and the elastic energy simplifies to<sup>26</sup>

$$E_{el} = \frac{1}{2} \int d^2\vec{r} \left( \lambda (u_{ii})^2 + 2\mu u_{ij}^2 \right), \quad (2)$$

and we assume summation over pairs of repeated indices.

A planar five-fold disclination defect can be constructed by removing a  $60^\circ$  angular section of a triangular lattice and sewing the two cut edges together. During such a deformation, all points move along an arc traversing a path of length  $\propto r$ , where  $r$  is the radial distance from the disclination. In other words, the displacement field produced by a five-fold disclination has a magnitude  $|\vec{u}(\vec{r})| \propto |\vec{r}|$  resulting in a constant strain field,  $u_{ij}(\vec{r}) = \text{const.}$  This observation immediately leads to the estimate of the stretching energy,

$$E_{el}^{(5)} \sim R^2, \quad (3)$$

where  $R$  is the disclination radius. A detailed calculation<sup>27</sup> finds  $E_{el}^{5-fold} = (Y/32\pi) R^2$ , where  $Y$  is the two-dimensional Young's modulus.

If the disclination is allowed to buckle out of its plane it can lower its energy by forming a conical structure with the apex at the disclination. In this case, the stretching energy is relieved at the expense of a bending penalty. The bending penalty is given by<sup>27,28</sup>

$$E_{bend} = \int dS (2\kappa H^2 + \kappa_G K). \quad (4)$$

If the boundary of the integration domain does not change during buckling, the Gauss-Bonnet theorem<sup>29</sup> ensures that the Gaussian curvature term does not contribute to the energy and one needs to retain only the mean curvature contribution. For a cone one of the principal curvature directions is along its slant height (i.e.,  $\kappa_1 = 0$ ) while the other is perpendicular to it (i.e.,  $\kappa_2 \propto 1/r$ , with  $r$  being the distance from the apex). Therefore, we immediately obtain,  $H \propto \frac{1}{r}$ , leading to the estimate for the bending energy

$$E_{bend}^{(5)} \sim \log(R/a), \quad (5)$$

where  $a$  is some microscopic length scale of the order of the lattice spacing. A detailed calculation<sup>27</sup> finds  $E_{bend}^{(5)} \approx (\pi/3) \kappa \log(R/R_b) + \frac{1}{32\pi} Y R_b^2$ , where  $R_b \approx \sqrt{154\kappa/Y}$ . By comparing Eqs. (3) and (5) it is clear that for small radii, the elastic stretching energy will be smaller than bending energy and the disclination will remain flat at the expense of stretching its surrounding. As  $R$  increases, the logarithm grows less rapidly than  $R^2$  and it becomes

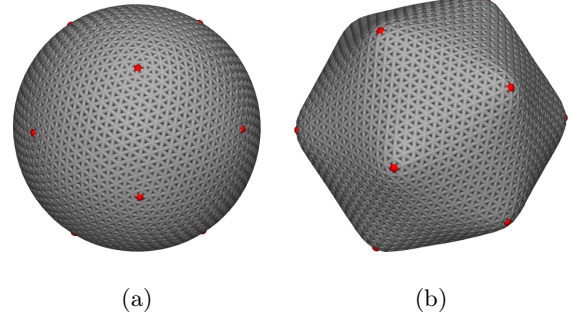


Figure 1: Disclination-driven buckling into an icosahedron. The transition is triggered if the dimensionless FvK number  $\gamma$  exceeds a critical value  $\gamma \sim 10^2$ .<sup>30</sup> Simulated structures are constructed using  $(p, q) = (12, 3)$   $T$ -number triangulation with  $\approx 2 \times 10^3$  vertices and radius  $R \approx 11.5l_0$ , with  $l_0 = 1$  being the average lattice spacing. (a)  $\gamma \approx 170$  and (b)  $\gamma \approx 3500$ . Red dots designate five-fold defects. All snapshots are generated with the Visual Molecular Dynamics (VMD) package<sup>31</sup> and rendered with the Tachyon ray-tracer.<sup>32</sup>

energetically favorable to buckle into a cone. A detailed calculation<sup>27</sup> shows that the buckling transition occurs if the dimensionless ratio, the so called Föppl-von Kármán or FvK number,  $\gamma = \frac{Y R^2}{\kappa} \gtrsim 154$ .

Another consequence of their non-local character is that disclination defects, much like charges, exert long-range forces on each other. This long-range force is transmitted via elastic deformation of the medium with the speed of sound playing the role of the speed of light in electrostatics. Disclinations with the same topological charge ( $s = 1$  for a five-fold defect) repel each other. Therefore, on a sphere disclinations take a configuration that maximizes their separation, which is an icosahedron for twelve defects.<sup>25</sup>

Moving from the planar to spherical geometry does not change the functional forms of the stretching and bending energies, albeit renormalizes numerical prefactors due to partial screening of the strain induced by the non-zero Gaussian curvature of the sphere.<sup>25</sup> As in the planar case, therefore, the onset of buckling solely depends on the relative strengths of stretching and bending energies. Since the stretching energy rapidly grows with the radius of the sphere once a critical value is reached all defects simultaneously buckle into cones thus forming an icosahedral vesicle.<sup>30</sup> In Fig. 1 we show the shape of the shell below and above the buckling transition. The transition is not sharp but a rounded smooth crossover, with vesicles having the FvK number  $\gamma \lesssim 150$  being spherical, for  $200 \lesssim \gamma \lesssim 1500$  being noticeably buckled, and for  $\gamma \gtrsim 2000$  being very sharp. For extremely large FvK numbers ( $\gamma \gtrsim 10^7$ ) the vesicle is non-extensible and one observes a characteris-

tic ridge-like structures with very interesting scaling properties, e.g.,  $E_{ridge}/\kappa \sim \alpha^{7/3} (YL^2/\kappa)^{1/6}$ , where  $\alpha$  is the angle of the ridge and  $L$  is its length.<sup>33,34</sup>

Finally, we note that imposing internal pressure<sup>35</sup> or a volume constraint<sup>35,36</sup> does not qualitatively affect the buckling transition but shifts its onset to higher values of  $\gamma$ .

### B. Buckling of multicomponent vesicles

An implicit assumption in the discussion thus far has been that the vesicle is made of an elastically homogenous material. Introducing heterogeneities by allowing for spatially varying Young's modulus and bending rigidity can lead to an alternative buckling mechanism. For example, presence of heterogeneities is believed to be responsible for the structure of recently synthesized assemblies of oppositely charged amphiphiles.<sup>6,8</sup> Observed structures are  $\sim 100\text{nm}$  size bilayer vesicles that are faceted but not icosahedral. SAXS/WAXS measurements combined with atomistic and semi-atomistic molecular dynamics simulations have revealed the existence of strongly correlated crystalline domains within the bilayer.<sup>8</sup> A typical domain size was found to be  $\approx 25\text{nm}$ . Simulations show that the crystalline orders of two neighboring domains are not mutually aligned and that the domains are separated by narrow regions of disordered, or even liquid, amphiphiles. It is reasonable to expect that the bilayer will be softer along those disordered boundary regions. These regions represent grain boundary defects with very different physical properties from the topological defects discussed in the previous section.

In order to model a vesicle with inhomogeneous elastic parameters we generalize the expressions for stretching (Eq. (2)) and bending (Eq. (4)) energies and allow the two Lamé coefficients and the bending rigidity to depend on the spatial position, i.e.,  $\lambda = \lambda(\vec{r})$ ,  $\mu = \mu(\vec{r})$ , and  $\kappa = \kappa(\vec{r})$ . For simplicity we assume that each of these coefficients can take only two values, denoted as “hard” and “soft” and loosely corresponding to strongly correlated facets and grain boundary regions, respectively.

The elasticity theory of thin objects is non-linear<sup>37</sup> and if one allows for spatially varying elastic parameters (even if they have a simple binary distribution) it quickly becomes analytically intractable. It is necessary to devise a scheme that allows us to obtain low energy states of the system using numerical simulations. The vesicle is represented as a discrete triangulated surface. In the case of modeling viral capsids, the vertices of the triangulation correspond to individual capsomeres. If the constitutive units are smaller, as is the case for amphiphilic vesicles, the

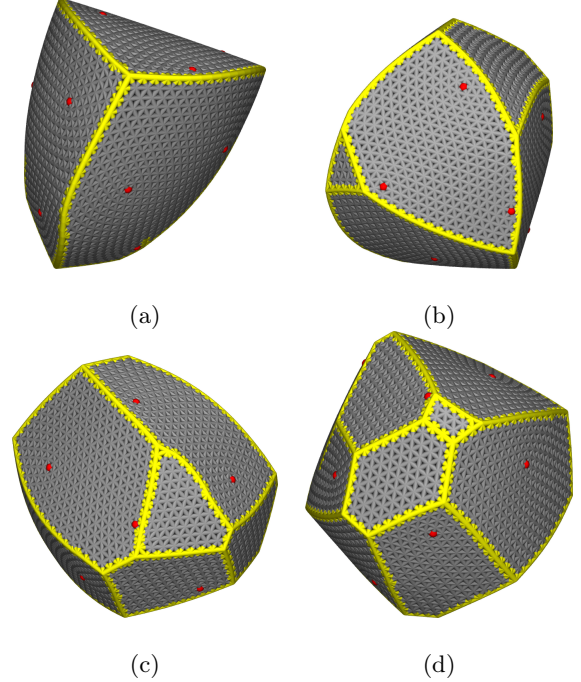


Figure 2: Snapshots of faceted structures with 3% (a), 4% (b), 4.5% (c), and 5% (d) of the soft component (yellow). Twelve five-fold dislocation defects are present as required by the spherical topology but appear to have no influence on the position of the edges and size of facets.

triangulation can be thought of as a coarse-graining scheme that assigns discrete elements to the patches of actual molecules. Each patch is large enough to contain a sufficient number of microscopic degrees of freedom that molecular details are of no importance but small enough to be considered homogeneous.

On a triangular lattice the simplest form of a discrete stretching energy for a multicomponent system can be obtained if we assume that the neighboring sites are connected to each other with harmonic springs with spatially-dependent spring constants  $\varepsilon_{ij}$  and a uniform rest length  $l_0$ <sup>27</sup>

$$\tilde{E}_{el} = \frac{1}{2} \sum_{\langle i,j \rangle} \varepsilon_{ij} (l_{ij} - l_0)^2, \quad (6)$$

where  $l_{ij} = |\vec{r}_i - \vec{r}_j|$  is the Euclidean distance between sites at  $\vec{r}_i$  and  $\vec{r}_j$ ,  $\varepsilon_{ij} \in \{\varepsilon_{hard}, \varepsilon_{soft}\}$ , and the sum is carried out over all pairs of nearest neighbors. It is convenient to set  $l_0 = 1$  and use it as a unit of length.

A proper discretization of the bending energy is more complicated with a number of approaches proposed in physics, applied mathematics, and computer graphics literature.<sup>27,38–41</sup> Different approaches vary in the level of computational complexity and accuracy. For the present discussion it is suf-



ficient to adopt the simple discretization suggested by Seung and Nelson.<sup>27</sup> The discrete bending energy is computed as

$$\begin{aligned}\tilde{E}_{bend} &= \frac{1}{2} \sum_{\langle I, J \rangle} \tilde{\kappa}_{IJ} (\vec{n}_I - \vec{n}_J)^2 \\ &= \sum_{\langle I, J \rangle} \tilde{\kappa}_{IJ} (1 - \cos(\theta_{IJ})),\end{aligned}\quad (7)$$

where  $\theta_{IJ}$  is the angle between unit-length normals  $\vec{n}_I$  and  $\vec{n}_J$  to the neighboring triangles  $I$  and  $J$ , and  $\tilde{\kappa}_{IJ}$  is the position dependent discrete bending rigidity also picked from a binary set  $\{\kappa_{hard}, \kappa_{soft}\}$ . The spring constant and the discrete bending rigidity are related to the Young's modulus and bending rigidity of the continuum theory by  $Y = 2\varepsilon/\sqrt{3}^{27}$  (with Poisson's ratio  $\nu = 1/3$ ) and  $\kappa = \sqrt{3}\tilde{\kappa}/2$ .<sup>27,42</sup>

Unlike single component systems where only shape changes are allowed, thus rendering standard numerical minimization techniques (e.g., conjugate-gradient minimization) applicable, for multicomponent vesicles it would be beneficial to have a strategy that simultaneously optimizes shape and the component arrangement. This can be achieved by using stochastic minimization techniques, e.g., the simulated annealing Monte Carlo method. Two components are assigned at random to vertices (or equivalently to edges or triangles) of the initial sphere such that the total fraction of the soft component is  $f$ . A Monte Carlo move consists of two stages: 1) a vertex is displaced by a vector  $\Delta\vec{r}$  with components chosen at random from a uniform distribution in an interval  $[-\zeta l_0, \zeta l_0]$  (typically,  $\zeta \approx 0.05$ ) followed by 2) swap of types (soft $\leftrightarrow$ hard) of a pair of randomly selected vertices. In both stages moves are accepted according the Metropolis rules. During a simulation, various cooling protocols can be applied, e.g. linear, exponential, power-law, etc. We note that the annealing temperature is not the actual physical temperature (characteristic energy scales in real vesicles significantly exceed  $k_B T$  and thermal fluctuations can be ignored; however an interesting example where this is not the case has recently been discussed<sup>43</sup>) but rather a parameter that controls the rate at which Monte Carlo moves that increase energy are accepted. During the component swap stage the total fraction of each component is kept fixed, i.e., no moves that would transform type of a vertex, e.g., from being hard to being soft, are allowed. Finally, the component swap move does not correspond to an actual rearrangement of the material within the vesicle - the vesicle is assumed to be solid and no diffusion is allowed, but is a convenient simulation tool that allows sampling of the space of component arrangements. Throughout a simulation the triangulation is preserved, i.e., no edge-flip

moves<sup>44</sup> that would create or annihilate defects are allowed.

The main drawback of the simulated annealing approach is that it typically converges very slowly once a minimum has been approached (for studied system sizes a minimum is typically reached after  $10^5 - 10^6$  Monte Carlo sweeps) and there is no guarantee that the obtained structure is true a global minimum, i.e., the ground state configuration. Therefore, we refer to the obtained shapes as *typical*. Ultimately, there is no reason to expect that the experimentally observed shapes correspond to the equilibrium structures. The realized shape will depend on the details of the assembly process in ways that are at present not understood.

A detailed study<sup>45</sup> of the shapes of two component elastic vesicles has found a wide variety of regular and irregular polyhedral shapes, some of which are shown in Fig. 2. If a small amount of soft component is added to an otherwise hard vesicle it arranges into branching lines. As the amount of the soft component is increased, these lines start to merge and form facets. Facets are nearly flat with very sharp bends along the soft ridges. The total number of facets increases with the amount of the soft component until a non-universal, size-dependent concentration is reached. Beyond this size-dependent concentration of the soft component it is no longer favorable to generate new facets but instead the soft component is randomly distributed inside the existing ones. Although each configuration still contains twelve five-fold defects, it appears that the size of the facets and the position of the soft ridges is not sensitive to their presence (Fig. 2). We point out that it is possible to entirely remove the residual strain induced by the defects either by appropriately tuning the spring rest lengths<sup>46</sup> or by directly working with reference and realized metrics.<sup>47,48</sup> Such an approach<sup>49</sup> shows that indeed faceting of the soft-hard two component vesicles occurs even if the defect contribution to the elastic energy is removed.

Thus far we have not assumed any mixing penalty for the two components. The components segregated solely as a result of the bending preference. If a mixing penalty, i.e., an effective line tension,  $\Gamma$ , is introduced it competes with the organization of the components that is preferred by elasticity and leads to an even richer variety of shapes.<sup>50</sup> For a weak line tension elasticity dominates and the soft component forms highly bent ridges separating flat hard faces. The width of these soft ridges grows as the line tension increases. If  $\Gamma$  is increased even further, the faces start to coarsen and merge together, until the components fully separate at  $\Gamma l_0/\kappa_{hard} \approx 10^{-2}$ ,<sup>50</sup> suggesting that even a small amount of mixing penalty can lead to full phase segregation. A

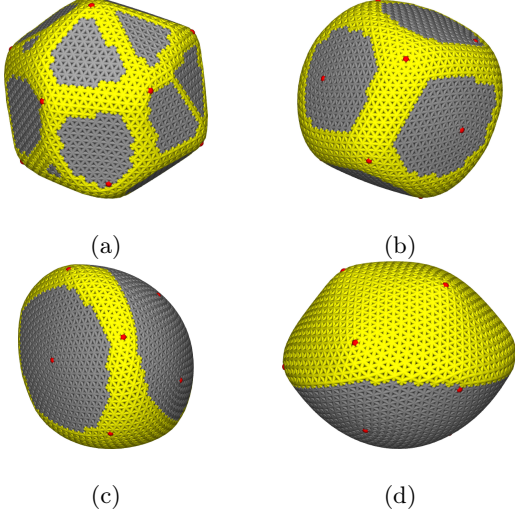


Figure 3: Snapshots of faced elastic vesicles with various mixing penalties between soft (yellow) and hard (gray) components for a system with an equal amount of hard and soft vertices. Mixing penalty increases from (a) to (d).

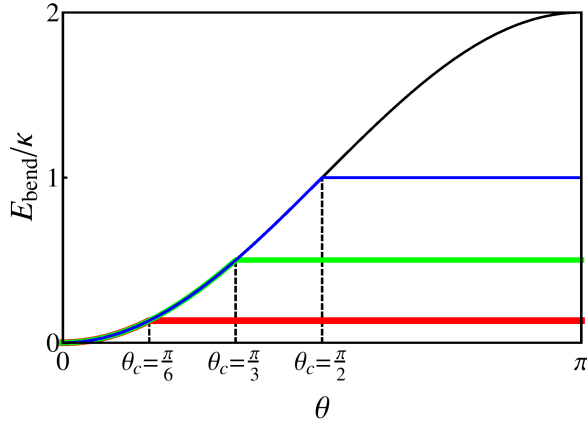


Figure 4: Bending energy (in units of the bending rigidity  $\kappa$ ) as a function of the angle  $\theta$  between unit-length normals to two neighboring triangles without a critical angle (black), with  $\theta_c = \frac{\pi}{6}$  (red), with  $\theta_c = \frac{\pi}{3}$  (green), and with  $\theta_c = \frac{\pi}{2}$  (blue).

subset of shapes of two-component vesicles with line tension is shown in Fig. 3.

We note that line tension can lead to very interesting shapes in two-<sup>51</sup> and three-component liquid vesicles.<sup>52</sup>

### C. Faceting due to critical curvature

Some of the faceted shapes observed in experiments as well as those obtained in simulations (e.g.,

Fig. 2) show sharp ridges with a large dihedral angle between neighboring facets. Once the radius of curvature becomes comparable with the molecular length scales the deformation is no longer locally small and microscopic details of the vesicle start to play a role. Eq. (7) was derived<sup>27</sup> under the assumption that curvature is smooth and slowly varying between neighboring points, such the bending energy could be expanded in terms of small deviations of the normal vectors to a planar surface and only leading terms retained. For a locally large deformation this is no longer justifiable and the expression for the bending energy needs to be modified. This is clearly a very hard problem that requires a detailed knowledge of the microscopic structure of the vesicle wall. Instead of constructing such a detailed model, we make a simple assumption that beyond a critical angle bending energy saturates. In other words, Eq. (7) is modified to

$$\tilde{E}_{bend}^{crit} = \tilde{\kappa} \sum_{\langle I, J \rangle} (1 - F(\theta_{IJ})), \quad (8)$$

where

$$F(\theta) = \begin{cases} \cos(\theta) & \text{for } \theta \leq \theta_c \\ \cos(\theta_c) & \text{for } \theta > \theta_c \end{cases} \quad (9)$$

and as in Eq. (7)  $\theta_{IJ}$  measures the angle between normals to a pair of neighboring triangles and  $\theta_c$  is the critical value of that angle beyond which the bending penalty saturates. Plot of the  $\tilde{E}_{bend}^{crit}$  vs.  $\theta$  is shown in Fig. 4. In this model  $\theta_c$  is treated as an input parameter. In essence,  $\theta_c$  controls the deformation angle beyond which the vesicle wall is sufficiently deformed that atomistic details start to be important. We assume that the vesicle is homogenous sphere with uniform values for  $\tilde{\kappa}$  and  $\varepsilon$ , and a standard triangular lattice with twelve five-fold defects positioned at the corners of an inscribed icosahedron. While one could easily argue that the stretching energy would also need to be modified, for simplicity, we use the expression in Eq. (6) and note that test simulations show that the results are not qualitatively affected by this simplification. As before, the low energy states were found using simulated annealing Monte Carlo simulations. No constraints on volume or area were imposed. Minimum energy configurations were found within  $\approx 10^6$  Monte Carlo sweeps using a linear cooling protocol.

We studied vesicles with  $\approx 6 \cdot 10^3$  vertices ( $(p, q) = (18, 10)$ - chiral;  $(25, 0)$ - achiral) over a range of values of the FvK number ( $\gamma$ ) and critical angle ( $\theta_c$ ). In Fig. 5 we show a phase diagram of this system mapped with  $\approx 200$  independent pairs of  $\gamma$  and  $\theta_c$ . Five distinct regimes are identified. For low values of  $\gamma$  and moderate to large  $\theta_c$  (green region, denoted as

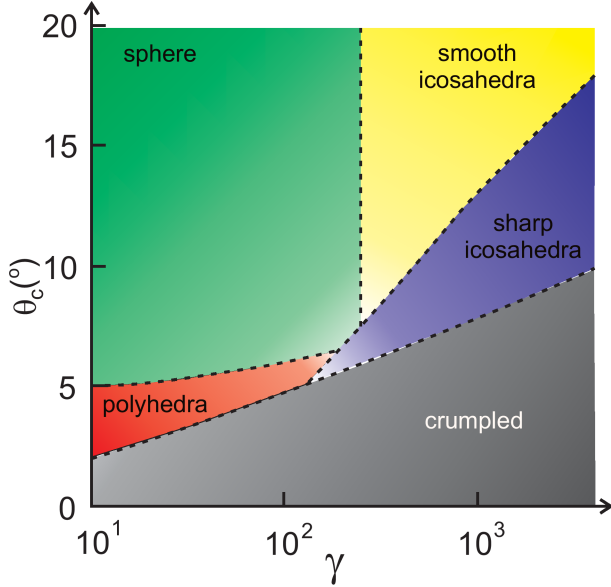


Figure 5: Phase diagram for a vesicle with critical bending angle as a function of the FvK number ( $\gamma$ ) and the value of the critical angle ( $\theta_c$ , shown in degrees). We identify five distinct regimes. In the “sphere” (green) and “smooth icosahedra” (yellow) regimes  $\theta_c$  is large and does not affect the shape. For small  $\gamma$  the vesicle is spherical and crosses over into a smooth icosahedron as  $\gamma$  is increased. At lower values of  $\theta_c$  the presence of critical angle starts to play a role and the vesicle shape changes substantially. For small  $\gamma$  elastic energy is completely dominated by the bending contribution and the vesicle takes shapes of irregular polyhedra (red region). For larger values of  $\gamma$  stretching energy caused by topological defects cannot be ignored and the icosahedral symmetry reemerges, but accompanied by sharp ridges (blue region). Finally, for very small values of  $\gamma$  the vesicle is unstable and crumples (gray).

“sphere” in Fig. 5) bending penalty is too large and the vesicle prefers to remain spherical. In this regions, angles between normals on any pair of neighboring triangles are smaller than  $\theta_c$  and the existence of an angle cutoff plays no role on the shape. In other words, we recover the situation discussed in Section II A. If  $\gamma$  is increased while keeping  $\theta_c$  large, one crosses over into the regime where icosahedral shapes are favorable. Since no deformation exceeds  $\theta_c$  the transition occurs at the same value of  $\gamma$  as in the case without the critical bending angle (yellow region, denoted as “smooth icosahedra” in Fig. 5). If  $\theta_c$  is reduced the effects of the angle cutoff start to emerge affecting the low energy shapes. In the region where  $\gamma$  is small (red region denoted as “polyhedra” in Fig. 5) one observes irregular polyhedra with sizes and positions of facets and edges that are insensitive to the presence of the five-fold defects. This is to be expected as for small  $\gamma$  bending penalty com-

pletely dominates over stretching and defect-driven buckling into a cone is suppressed. In this region faceting mechanism is similar to the buckling as the soft component discussed in the previous section. As  $\gamma$  is increased the topological defects start to play the role and the system transitions in the regime where they drive buckling. With a relatively small value of  $\theta_c$ , however, the system can further lower its energy by forming sharp edges that emanate from the defects. This region is denoted as “sharp icosahedra” (blue in Fig. 5). We note that the direction of the sharp edges appears to depend on the details of the triangulation. Finally, if  $\theta_c$  is too small the vesicle becomes unstable and crumples (gray region denoted as “crumpled” in Fig. 5). In this region, the simulations often fail to converge and instead get locked in high-energy states that often occur in the early stages of a simulation. In Fig. 6 we show typical low energy configurations in each of the five regimes.

### III. SUMMARY AND CONCLUSIONS

We have showed that faceted structures can be low energy configurations of elastic vesicles as a result of a number of different mechanisms. Incompatibility between crystalline order and spherical topology leads to the presence of topological defects resulting in a residual stress even in the ground state. The stress can be in part relieved by buckling into cones seeded at the defects. Due to the high symmetry of the ground state distribution of the defects, the buckled structure is an icosahedron. This mechanism can qualitatively account for the observation that smaller icosahedral viruses (e.g. *Polyomaviruses*<sup>53</sup>) are smooth (spherical) while larger viruses (e.g. *Mimivirus*<sup>54</sup>) are buckled. For viruses the size of each capsomer is sufficiently large ( $\sim 10\text{nm}$ ) that the capsid is a nearly perfect lattice with  $\sim 10^2 - 10^3$  units and no additional defects beyond the minimum twelve five-fold sites required by the topology. In case of lipid bilayer vesicles lipid molecules are much smaller (occupying an area  $\lesssim 0.5\text{nm}^2$ ) and each vesicle is assembled from hundreds of thousands of lipids. If a crystal is formed on such a vesicle as a result of cooling or strong electrostatic correlations it is much harder to form a perfect lattice and one instead expects grain boundaries to form. This effect is even enhanced by the spherical topology that hinders formation of a uniform crystal to begin with. In the grain boundary region molecules are disordered and may even be in the liquid state. As a result, the wall is expected to be softer. We have shown that if one allows for the presence of softer component in an otherwise crystalline vesicle, the low energy config-

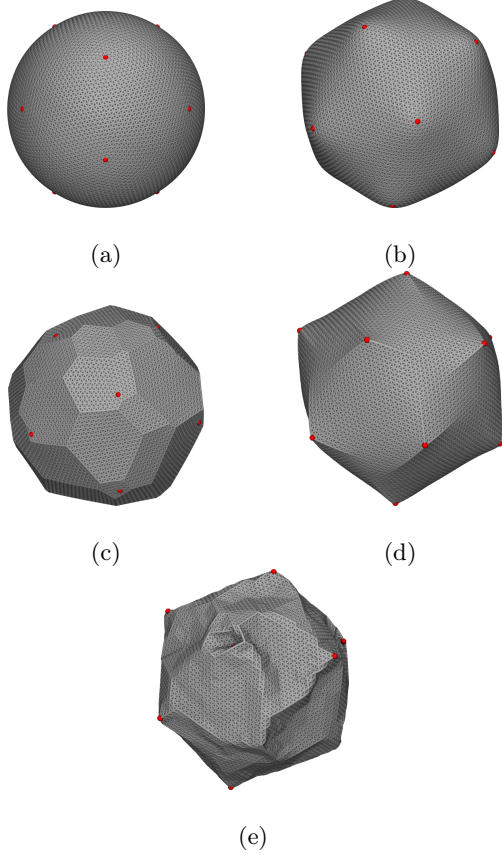


Figure 6: Snapshots of the low energy configurations of a vesicle constructed using  $(p, q) = (18, 10)$   $T$ -number triangulation with  $\approx 6 \times 10^3$  vertices and radius  $R \approx 20.5l_0$ . (a) For low a FvK number  $\gamma \approx 50$  and a large critical angle  $\theta_c = 20^\circ$  the vesicle remains spherical. (b) For  $\gamma \approx 10^3$  and  $\theta_c = 20^\circ$  one observes a smooth buckled structure with icosahedral symmetry akin to the shapes discussed in Section II A. (c) For small  $\gamma \approx 60$  and small  $\theta_c = 5^\circ$  we find an irregular polyhedral vesicle with facets being insensitive to the position of the defects. (d) As FvK number if increased to  $\gamma \approx 10^3$  and the critical angle set to  $\theta_c = 14^\circ$  the structure is icosahedral but with sharp ridges emanating for each defect. (e) Finally, at  $\gamma \approx 2.5 \cdot 10^3$  and very small critical angle,  $\theta_c = 2^\circ$  the vesicle is no longer stable and crumples. Red points indicate positions of twelve five-fold defects.

uration can be regular and irregular polyhedra that are not icosahedra. The soft component forms ridges that are highly bent and separate hard flat facets. The faceting mechanism is distinctly different from the buckling into an icosahedron seeded at the five-fold sites. Furthermore, it is reasonable to expect that the bending response of the vesicle wall is not linear and significantly changes if the local deformation becomes large. We introduced a simple model that takes into account such effects at the most basic level. Even with a such simplified model we were able to show that a non-linearity in the bending response can drastically affect the low energy shapes and lead to interesting faceted structures.

Understanding the mechanisms that lead to faceting of vesicles goes beyond the realm of an academic exercise and could have a far-reaching impact on nano-technology. For example, flat faces could be easier to functionalize or otherwise chemically treat. Biochemical reactions are expected to have different rates near flat compared to curved surfaces, which could be utilized to construct highly sensitive transport agents. With the ability to accurately control the shape of vesicles it could be possible to engineer vesicles that would, e.g., selectively target only particular agents. We hope this work will broaden the interest in this emergent subject of modern nanoscience.

This work was supported by NSF grant DMR-0808812. RS would like to thank M. Demers, C. Funkhouser, C. Leung, M. Olvera de la Cruz, L. Palmer, B. Qiao, and G. Vernizzi for collaborations on various aspects of the study of faceting in multicomponent vesicles as well as to R. Everaers who suggested to analyze effects of critical angle bending. RS tanks the Soft Matter Program at Syracuse University for financial support.

\* Electronic address: bowick@phy.syr.edu

† Electronic address: sknepnek@gmail.com

<sup>1</sup> C. V. Iancu, D. M. Morris, Z. Dou, S. Heinhorst, G. C. Cannon, and G. J. Jensen, *Journal Of Molecular Biology* **396**, 105 (2010).

<sup>2</sup> A. Walsby, *Nature* **283**, 69 (1980).

<sup>3</sup> A. Blaurock and R. Gamble, *Journal of Membrane Biology* **50**, 187 (1979).

<sup>4</sup> E. Marques, O. Regev, A. Khan, M. da Graca Miguel, and B. Lindman, *Macromolecules* **32**, 6626 (1999).

<sup>5</sup> F. Antunes, R. Brito, E. Marques, B. Lindman, and M. Miguel, *The Journal of Physical Chemistry B* **111**, 116 (2007).

<sup>6</sup> M. A. Greenfield, L. C. Palmer, G. Vernizzi, M. Olvera de la Cruz, and S. I. Stupp, *Journal of the American Chemical Society* **131**, 12030 (2009).

<sup>7</sup> M. Dubois, B. Deme, T. Gulik-Krzywicki, J.-C. Dedieu, C. Vautrin, S. Desert, E. Perez, and T. Zemb, *Nature* **411**, 672 (2001).

<sup>8</sup> C. Leung, L. Palmer, B. Qiao, S. Kewalra-

- mani, R. Sknepnek, C. Newcomb, M. Greenfield, G. Vernizzi, S. Stupp, M. Bedzyk, *et al.*, ACS Nano **6**, 10901 (2012).
- <sup>9</sup> L. Jia, A. Cao, D. Lévy, B. Xu, P. Albouy, X. Xing, M. Bowick, and M. Li, Soft Matter **5**, 3446 (2009).
  - <sup>10</sup> B. Xu, R. Piñol, M. Nono-Djamen, S. Pensec, P. Keller, P. Albouy, D. Lévy, and M. Li, Faraday discussions **143**, 235 (2009).
  - <sup>11</sup> L. Jia, D. Lévy, D. Durand, M. Impérator-Clerc, A. Cao, and M. Li, Soft Matter **7**, 7395 (2011).
  - <sup>12</sup> L. Lamb, D. Huffman, R. Workman, S. Howells, T. Chen, D. Sarid, and R. Ziolo, Science **255**, 1413 (1992).
  - <sup>13</sup> M. Hu, J. Chen, M. Marquez, Y. Xia, and G. V. Hartland, Journal of Physical Chemistry C **111**, 12558 (2007).
  - <sup>14</sup> B. Alberts, A. Johnson, J. Lewis, M. Raff, K. Roberts, and P. Walter, *Molecular Biology of the Cell* (Garland Science, New York, 2002).
  - <sup>15</sup> A. Bangham and R. Horne, Journal of molecular biology **8**, 660 (1964).
  - <sup>16</sup> S. Veatch and S. Keller, Biophysical Journal **85**, 3074 (2003).
  - <sup>17</sup> C. Nardin, T. Hirt, J. Leukel, and W. Meier, Langmuir **16**, 1035 (2000).
  - <sup>18</sup> W. Helfrich, Zeitschrift Fur Naturforschung C-a Journal Of Biosciences **C 28**, 693 (1973).
  - <sup>19</sup> S. Munro, Cell **115**, 377 (2003).
  - <sup>20</sup> T. A. Witten, Rev. Mod. Phys. **79**, 643 (2007).
  - <sup>21</sup> A. González-Pérez, M. Schmutz, G. Waton, M. Romero, and M. Krafft, Journal of the American Chemical Society **129**, 756 (2007).
  - <sup>22</sup> C. A. Haselwandter and R. Phillips, Phys. Rev. Lett. **105**, 228101 (2010).
  - <sup>23</sup> D. L. D. Caspar and A. Klug, Cold Spring Harbor Symposia on Quantitative Biology **27**, 1 (1962).
  - <sup>24</sup> S. Sachdev and D. R. Nelson, J. Phys. C: Solid State Phys. **17**, 5473 (1984).
  - <sup>25</sup> M. Bowick, D. Nelson, and A. Travesset, Physical Review B **62**, 8738 (2000).
  - <sup>26</sup> L. Landau and E. Lifshitz, *Theory of Elasticity*, 3rd ed. (Butterworth-Heinemann, London, 1995).
  - <sup>27</sup> H. S. Seung and D. R. Nelson, Physical Review A **38**, 1005 (1988).
  - <sup>28</sup> W. Koiter, *A consistent first approximation in the general theory of thin elastic shells: Foundations and linear theory*, pt. 1 (Laboratorium voor Toegepaste Mechanica der Technische Hogeschool, 1959).
  - <sup>29</sup> M. Do Carmo, *Differential geometry of curves and surfaces*, Vol. 1 (Prentice-Hall Englewood Cliffs, NJ, 1976).
  - <sup>30</sup> J. Lidmar, L. Mirny, and D. R. Nelson, Physical Review E **68**, 051910 (2003).
  - <sup>31</sup> W. Humphrey, A. Dalke, and K. Schulten, Journal of Molecular Graphics **14**, 33 (1996).
  - <sup>32</sup> J. Stone, *An Efficient Library for Parallel Ray Tracing and Animation*, Master's thesis, Computer Science Department, University of Missouri-Rolla (1998).
  - <sup>33</sup> A. E. Lobkovsky, Phys. Rev. E **53**, 3750 (1996).
  - <sup>34</sup> A. E. Lobkovsky and T. Witten, Physical Review E **55**, 1577 (1997).
  - <sup>35</sup> A. Siber, Physical Review E **73**, 061915 (2006).
  - <sup>36</sup> C. M. Funkhouser, R. Sknepnek, and M. Olvera de la Cruz, Soft Matter **9**, 60 (2012).
  - <sup>37</sup> B. Audoly and Y. Pomeau, *Elasticity and Geometry - From Hair Curls to the Non-linear Response of Shells* (Oxford University Press, Oxford, UK, 2010).
  - <sup>38</sup> K. Brakke, Experimental Mathematics **1**, 141 (1992).
  - <sup>39</sup> G. Gompper and D. Kroll, Journal De Physique I **6**, 1305 (1996).
  - <sup>40</sup> M. Meyer, M. Desbrun, P. Schröder, and A. H. Barr, Visualization and mathematics **3**, 34 (2002).
  - <sup>41</sup> E. Magid, O. Soldea, and E. Rivlin, Computer Vision and Image Understanding **107**, 139 (2007).
  - <sup>42</sup> B. Schmidt and F. Fraternali, Journal of the Mechanics and Physics of Solids **60**, 172 (2012).
  - <sup>43</sup> J. Paulose, G. A. Vliegenthart, G. Gompper, and D. R. Nelson, Proceedings of the National Academy of Sciences **109**, 19551 (2012).
  - <sup>44</sup> D. Nelson, T. Piran, and S. Weinberg, *Statistical mechanics of membranes and surfaces*, 2nd ed. (World Scientific Singapore, 2004).
  - <sup>45</sup> G. Vernizzi, R. Sknepnek, and M. de la Cruz, Proceedings of the National Academy of Sciences **108**, 4292 (2011).
  - <sup>46</sup> E. Katifori, S. Alben, E. Cerda, D. R. Nelson, and J. Dumais, Proceedings of the National Academy of Sciences **107**, 7635 (2010).
  - <sup>47</sup> A. Green and W. Zerna, *Theoretical elasticity* (Dover Pubns, 2002).
  - <sup>48</sup> E. Efrati, E. Sharon, and R. Kupferman, Journal of the Mechanics and Physics of Solids **57**, 762 (2009).
  - <sup>49</sup> R. Sknepnek and M. Olvera de la Cruz, Physical Review E **85**, 050501 (2012).
  - <sup>50</sup> R. Sknepnek, G. Vernizzi, and M. Olvera de la Cruz, Soft Matter **8**, 636 (2012).
  - <sup>51</sup> J. Hu, T. Weikl, and R. Lipowsky, Soft Matter **7**, 6092 (2011).
  - <sup>52</sup> M. F. Demers, R. Sknepnek, and M. O. de la Cruz, Physical Review E **86**, 021504 (2012).
  - <sup>53</sup> B. Sweet and M. Hilleman, in *Proceedings of the Society for Experimental Biology and Medicine. Society for Experimental Biology and Medicine* (New York, NY), Vol. 105 (Royal Society of Medicine, 1960) pp. 420–427.
  - <sup>54</sup> B. La Scola, S. Audic, C. Robert, L. Jungang, X. de Lamballerie, M. Drancourt, R. Birtles, J.-M. Claverie, and D. Raoult, Science **299**, 2033 (2003).